

# First *Gaia* dynamical model of the Milky Way disc with six phase space coordinates: a test for galaxy dynamics

Maria Selina Nitschai,<sup>1,2,3</sup> Michele Cappellari<sup>3</sup> and Nadine Neumayer<sup>2</sup>

<sup>1</sup>Heidelberg University, Seminarstraße 2, 69117 Heidelberg, Germany

<sup>2</sup>Max-Planck-Institut für Astronomie (MPIA), Königstuhl 17, D-69121 Heidelberg, Germany

<sup>3</sup>Sub-department of Astrophysics, Department of Physics, University of Oxford, Denys Wilkinson Building, Keble Road, Oxford OX1 3RH, UK

15 February 2022

## ABSTRACT

We construct the first comprehensive dynamical model for the high-quality subset of stellar kinematics of the Milky Way disc, with full 6D phase-space coordinates, provided by the *Gaia* Data Release 2. We adopt an axisymmetric approximation and use an updated Jeans Anisotropic Modelling method, which allows for a generic shape and radial orientation of the velocity ellipsoid, as indicated by the *Gaia* data, to fit the mean velocities and all three components of the intrinsic velocity dispersion tensor. The Milky Way is the first galaxy for which all intrinsic phase space coordinates are available, and the kinematics are superior to the best integral-field kinematics of external galaxies. This situation removes the long-standing dynamical degeneracies and makes this the first dynamical model highly over-constrained by the kinematics. For these reasons, our ability to fit the data provides a fundamental test for both galaxy dynamics and the mass distribution in the Milky Way disc. We tightly constrain the average total density logarithmic slope, in the radial range 3.6–12 kpc, to be  $\alpha_{\text{tot}} = -2.149 \pm 0.055$  and find that the dark halo slope must be significantly steeper than  $\alpha_{\text{DM}} = -1$  (NFW). The dark halo shape is close to spherical and its density is  $\rho_{\text{DM}}(R_{\odot}) = 0.0115 \pm 0.0020 \text{ M}_{\odot} \text{ pc}^{-3}$  ( $0.437 \pm 0.076 \text{ GeV cm}^{-3}$ ), in agreement with previous estimates. The circular velocity at the solar position  $v_{\text{circ}}(R_{\odot}) = 236.5 \pm 3.1 \text{ km s}^{-1}$  (including systematics) and its radial trends are also consistent with recent determinations.

**Key words:** Galaxy: disc – Galaxy: kinematics and dynamics – Galaxy: solar neighbourhood

## 1 INTRODUCTION

For decades astrophysicist have constructed dynamical models of external galaxies from observations of their unresolved stellar kinematics to study their masses as well as their orbital and density distributions (see review by Courteau et al. 2014). The models were initially constrained by long-slit spectroscopy (e.g. van der Marel 1991) and nowadays by integral-field spectroscopy (see review by Cappellari 2016).

When using only projected line-of-sight kinematics and the first two velocity moments, there are well-known fundamental degeneracies between the mass density and the orbital distribution, or anisotropy, for spherical galaxies. This mass-anisotropy degeneracy (Binney & Mamon 1982; Gerhard 1993) led to the development of techniques to extract the elusive shape of the stellar line-of-sight velocity distribution from the galaxy spectra (e.g. van der Marel & Franx 1993) together with dynamical modelling approaches that could use that information to break the degeneracy (e.g.

Rix et al. 1997; van der Marel et al. 1998; Gebhardt et al. 2000; Valluri et al. 2004; Cappellari et al. 2006).

The mass-anisotropy degeneracy is less severe in axial symmetry as one can observe different views of the velocity ellipsoid along different polar angles on the sky. However, degeneracies must still be expected because the data cube is a three dimensional observable which cannot uniquely constrain the three-dimensional distribution function in addition to the galaxy density distribution (see discussion in Sec. 3 of Valluri et al. 2004). Moreover, the surface-brightness deprojection is also strongly degenerate, unless the galaxy is edge-on (Rybicki 1987). Dynamical degeneracies are indeed observed even with state-of-the-art dynamical models and data (Krajnović et al. 2005; de Lorenzi et al. 2009).

Heroic attempts were made to break the dynamical degeneracies using proper motion measurements in addition to line-of-sight kinematics (e.g. van de Ven et al. 2006; Watkins et al. 2015), but these useful proof-of-concept studies had to

rely on data of relatively limited quality. Moreover, these studies are only possible for very few cases, where the full velocity information is available.

Now, for the first time, all these long-standing dynamical degeneracy issues disappear for the kinematics of the Milky Way from the *Gaia* mission (Gaia Collaboration et al. 2016), which are based on direct proper motion and radial velocities determinations for millions of individual stars: (i) one can now obtain all six phase-space coordinates (three spatial coordinates and three velocities), making the dimension of the observable larger than that of the distribution function, thus allowing for extra parameters like the density to be uniquely constrained; (ii) one now measures the true velocity moments, by direct summation, over many stars rather than having to infer them from integrated galaxy spectra; (iii) the stellar density is uniquely obtained without the need for a deprojection.

In this situation, unlike the case of every galactic dynamical model that has been constructed in the past half a century, dimensional arguments alone already imply that there is no guarantee that even general models will be able to fit simultaneously all the components of the kinematics unless the model assumptions are sufficiently accurate. This dataset then allows us to make a fundamental physical test, namely to verify whether a model based on the Newtonian equations of motion<sup>1</sup>, which was developed based on the motions on the scale of the Solar System, is able to accurately predict the average motions of the stars at the scale of our Galaxy,  $10^8$  times larger.

Here we attempt to construct a first axisymmetric dynamical model of the Milky Way kinematics. We use the new spherically-aligned Jeans Anisotropic Method (JAM<sub>sph</sub>, Cappellari 2019), which allows for general axial ratios for all three components of the velocity ellipsoid and a spherical orientation, as indicated by the *Gaia* data (Hagen et al. 2019; Everall et al. 2019). We want to test to what accuracy a relatively simple model can capture the richness of the *Gaia* kinematics. We additionally provide a description of the mass density distribution (and circular velocity) of the Milky Way at radii  $r \approx 3.6\text{--}12$  kpc.

The outline of this paper is as follows: In Section 2 we briefly present the *Gaia* DR2 dataset and introduce the Jeans model, including its required components in Section 3. We present the resulting JAM model and the Milky Way circular velocity curve in Section 4, before concluding in Section 5.

## 2 GAIA STELLAR KINEMATIC DATA

In April 2018 *Gaia* had its second data release (Gaia Collaboration et al. 2018a) (*Gaia* DR2), which contains the data collected during the first 22 months of its nominal mission lifetime. This gives for the first time a high-precision parallax and proper motion catalogue for millions of sources, supplemented by precise and homogeneous multi-band all-sky photometry and a large radial velocity survey at the bright ( $G < 13$ ) end (Gaia Collaboration et al. 2018b).

Some early dynamical models used subsets of the DR2

*Gaia* data to infer the shape and mass of the dark matter halo (Posti & Helmi 2019; Watkins et al. 2019; Wegg et al. 2019), the Galaxy velocity curve (Eilers et al. 2019) or its non-equilibrium features (Antoja et al. 2018). However, no study has yet attempted to construct a comprehensive model of the bulk of the *Gaia* DR2, namely the few millions of stars with high-quality full six-dimensional phase space coordinates. This is the goal of this paper.

We use kinematics derived with Bayesian distance estimates of Schönrich et al. (2019). We assume as distance to the Galactic center  $R_\odot = 8.2$  kpc (Abuter et al. 2019), a vertical displacement of the Sun from the midplane of  $z_\odot = 0.02$  kpc (Joshi 2007) and as solar velocities in cylindrical Galactic coordinates  $(U_\odot, V_\odot, W_\odot) = (-11.1$  (Schönrich et al. 2010),  $247.4$  (Abuter et al. 2019),  $7.2$  (Reid et al. 2009))  $\text{km s}^{-1}$ . The giant stars, which are the main contribution at distances larger than 1 kpc from the Sun, are selected based on their absolute magnitude  $M_G < 3.9$ , intrinsic colour  $(G_{BP} - G_{RP})_0 > 0.95$  and positive parallaxes with relative uncertainty  $\varpi/\epsilon_\varpi > 5$ . This sample contains about  $1.98 \times 10^6$  stars and covers a volume with extreme cylindrical coordinates  $3.65 < R < 12.02$  kpc,  $-2.52 < z < 2.50$  kpc and  $-15^\circ < \phi < 15^\circ$ , which is divided into  $(R, z)$  cells of  $200 \times 200$  pc. For each cell with at least 30 stars we calculated the median velocity and the velocity dispersion.

## 3 METHODS

### 3.1 Model for the Milky Way stellar luminosity density

The first component one needs to construct for a stellar dynamical model is the distribution of the tracer population, from which the kinematics was derived. Ideally, this would be extracted from the same *Gaia* dataset we use to derive the kinematics, but this kind of model is not (yet) available.

Therefore, we use the Milky Way stellar distribution from Jurić et al. (2008) derived from the number density of main sequence stars using data from the Sloan Digital Sky Survey (SDSS). However, we are ignoring the stellar halo component since it is quite uncertain and not as important since our data are mainly stars in the Milky Way disc.

The disc is decomposed into a sum of two exponential components, the thin and the thick disc. This allows for different scale lengths ( $L_{\text{thin}}, L_{\text{thick}}$ ) and heights ( $H_{\text{thin}}, H_{\text{thick}}$ ) for each component:

$$\rho_D(R, z, L, H) = \rho(R_\odot, 0) \exp\left(-\frac{R - R_\odot}{L} - \frac{|z|}{H}\right) \quad (1)$$

$$\rho_D(R, z) = \rho_D(R, z, L_{\text{thin}}, H_{\text{thin}}) + f \times \rho_D(R, z, L_{\text{thick}}, H_{\text{thick}}) \quad (2)$$

where  $\rho(R_\odot, 0)$  is the number density of stars in the solar neighbourhood, and the parameter  $f$  in equation (2) is the thick disc normalization relative to the thin disc. Our adopted values are the “bias corrected” parameters (Jurić et al. 2008):  $f = 0.12$ ;  $(L_{\text{thin}}, H_{\text{thin}}) = (2.6, 0.3)$  kpc and  $(L_{\text{thick}}, H_{\text{thick}}) = (3.6, 0.9)$  kpc.

The parameter  $\rho(R_\odot, 0)$  was originally derived as a number density from star counts by Jurić et al. (2008), but since we want to obtain meaningful stellar mass-to-light values ( $M_*/L$ ) we normalize the density (Jurić et al. 2008) in such

<sup>1</sup> Relativistic corrections are unimportant here

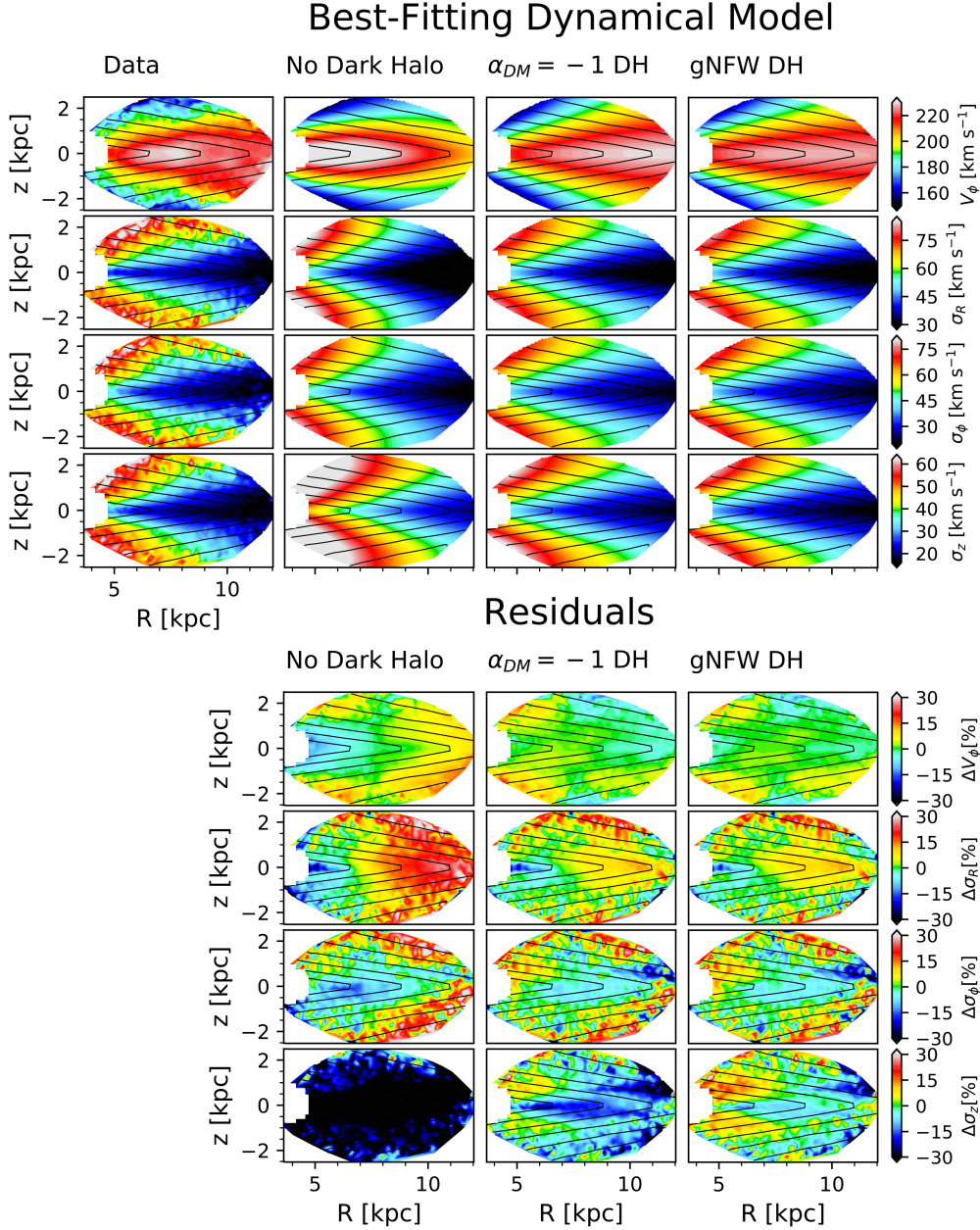


**Figure 1. Data versus models.** From left to right: (i) *Gaia* Data, (ii) best-fitting JAM<sub>sph</sub> model without dark matter, (iii) best model with a “standard” Navarro, Frenk and White (NFW) dark matter profile and (iv) the best-fitting model with gNFW halo profile, with free inner logarithmic slope. Below each model there are the residuals of them. From top to bottom the rows show the mean azimuthal velocity ( $v_\phi$ ), the radial ( $\sigma_R$ ), azimuthal ( $\sigma_\phi$ ) and vertical ( $\sigma_z$ ) velocity dispersions in the Galactic cylindrical coordinates.

a way that the stellar luminosity density at the solar radius corresponds to the local luminosity density in  $V$ -band  $\rho_L = 0.056 \text{ L}_\odot \text{V pc}^{-3}$ , which was derived in previous work of Flynn et al. (2006) using the local luminosity function and the vertical structure of the disc. We have chosen the  $V$ -band since the SDSS data, used to fit the disc model, and the *Gaia* data are including the  $V$ -band.

We further included the bulge, even though we have tested the sensitivity of our models to it and saw that it has a minimal effect on the disc area we are probing with the *Gaia* data and therefore we will keep it fixed for our

model. Even an extreme model without bulge would not affect our conclusions. We use a bulge model of McMillan (2017) which is an axisymmetric version of the one obtained from COBE/DIRBE photometry (Bissantz & Gerhard 2002):

$$\rho_b = \frac{\rho_{0,b}}{(1 + m/r_0)^a} \exp\left(-\frac{m^2}{r_{\text{cut}}^2}\right) \quad (3)$$

$$m^2 = R^2 + (z/q)^2. \quad (4)$$

We adopt the values of McMillan (2017)  $a = 1.8$ ,  $r_0 = 0.075$  kpc,  $r_{\text{cut}} = 2.1$  kpc and an axis ratio of  $q = 0.5$ . We normalize

the bulge to our disc by ensuring it has the same bulge to disc ratio as the original model (McMillan 2017), obtaining  $\rho_{0,b} = 80.81 \text{ L}_{\odot} \text{V pc}^{-3}$ .

Within 5 kpc from the Galactic center the bar dominates the kinematics (Wegg et al. 2015; Bovy et al. 2019) but since our data are mostly not covering this area we are ignoring the bar in our stellar model. The small fraction of stars that might belong to the bar with radii smaller than 5 kpc should not have a significant effect on our model. Previous studies showed that one can measure reliable quantities outside the bar region of barred galaxies (Lablanche et al. 2012), by symmetrizing the bar density as done here.

For use with our model, we approximate the intrinsic density of the disc + bulge stellar model with a multi-Gaussian expansion (MGE) (Emsellem et al. 1994; Cappellari 2002), by fitting a synthetic two-dimensional image using the MGE fitting method (Cappellari 2002) and `mgefit` software package<sup>2</sup>.

### 3.2 Model for the dark matter and gas contributions.

The second component of a dynamical model is the mass density of the Galaxy, which includes not only the stellar component but also the gas distribution and the dark matter halo.

We describe the dark matter as a generalized Navarro, Frenk and White profile (gNFW, Wyithe et al. 2001), with variable inner slope  $\alpha_{\text{DM}}$  and axial ratio  $q$ :

$$\rho_{\text{dm}} = \rho_s \left( \frac{m}{r_s} \right)^{\alpha_{\text{DM}}} \left( \frac{1}{2} + \frac{1}{2} \frac{m}{r_s} \right)^{-3-\alpha_{\text{DM}}}, \quad (5)$$

with  $m$  from equation (4) and where the scale radius is  $r_s$  is also allowed to vary between 10 and 26 kpc, consistent with values found with the prediction of the halo mass-concentration relation Navarro et al. (1996); Klypin et al. (2011)  $M_{200} - c_{200}$ , for a halo mass around  $M_{200} \approx 1.3 \times 10^{12} \text{ M}_{\odot}$  (Bland-Hawthorn & Gerhard 2016), and with actual measurements for the Milky Way (e.g. Eilers et al. 2019; McMillan 2017; Kafle et al. 2014).

If  $\alpha_{\text{DM}} = -1$ , equation (5) is the classical Navarro, Frenk and White (NFW) dark matter profile (Navarro et al. 1996). This 1-dimensional profile is fitted with Gaussians using the `mge_fit_1d` procedure in the `mgefit` package (see footnote 2), and appropriately made oblate/prolate, for use with the model.

In addition, we include the gas density, even though it is quite uncertain, again from the previous Milky Way model by McMillan (2017). We include the mass density of both the  $\text{H I}$  and  $\text{H}_2$  gas in the disc of the Milky Way (Eq. 4 in McMillan 2017). For simplicity, we ignore the hole in the centre of this density profile, which is outside the range of our kinematics, by removing the term in the equation that describes it, so that the gas model only declines exponentially towards larger  $r$ . The gas density is also fitted by creating an image which we fitted with `mgefit` (Cappellari 2002) as we did for the stellar model. This gas MGE will be added to the potential density of the Milky Way but will be kept fixed to

the quoted mass by McMillan (2017) during the model fit, since we just want it as an estimate of the mass contribution from the gas in the disc region.

### 3.3 Bayesian JAM modelling

For the dynamical modelling we use a new solution of the axisymmetric Jeans equations under the assumption of a spherically-aligned velocity ellipsoid (Cappellari 2019), which was shown to describing very accurately the dynamics of the *Gaia* data both in the outer halo (Wegg et al. 2019) and the disc region (Hagen et al. 2019; Everall et al. 2019). This JAM<sub>sph</sub> method was developed specifically with the *Gaia* data in mind. As an extreme test of the sensitivity of the model assumption on the orientation of the velocity ellipsoid, we also use for comparison the cylindrically-aligned JAM<sub>cyl</sub> solution and the `jampy` package<sup>3</sup>. The method solves the equations of stellar hydrodynamics (Jeans 1922) assuming axisymmetry and spherical alignment for the velocity ellipsoid while allowing for a variable anisotropy for each Gaussian component of the MGE (a three integral distribution function).

The JAM<sub>cyl</sub> method was applied to model the integral-field stellar kinematics of large numbers of external galaxies (see review in Cappellari 2016) and has been extensively tested against N-body simulations (Lablanche et al. 2012; Li et al. 2016) and in real galaxies against CO circular velocities (Leung et al. 2018), including many barred galaxies like the Milky Way. It was found to recover unbiased density profiles, even more accurately than the more general Schwarzschild (Schwarzschild 1979) approach (see Fig. 8 of Leung et al. 2018). A higher accuracy of JAM<sub>cyl</sub> with respect to Schwarzschild was confirmed (see Fig. 6 of Jin et al. 2019) using the currently state-of-the-art Illustris cosmological N-body simulation (Vogelsberger et al. 2014). Given its spherical alignment, the JAM<sub>sph</sub> method should be even more accurate for the Milky Way.

JAM<sub>sph</sub> gives the solution of the Jeans equations for all three mean velocity components ( $v_r, v_{\theta}, v_{\phi}$ ) and the velocity dispersion in the three directions (equations 52-54 of Cappellari 2019). We project the spherical velocities into cylindrical coordinates ( $v_R, v_{\phi}, v_z$ ). However, given that the model assumes a steady state,  $v_R$  and  $v_z$  are identically zero and do not need to be explicitly fitted. This assumption is consistent with good accuracy with the *Gaia* maps by Gaia Collaboration et al. (2018b) which also show these velocities to be small for the purpose of this study ( $-15 \lesssim v_R \lesssim 15 \text{ km s}^{-1}$ ,  $-10 \lesssim v_z \lesssim 10 \text{ km s}^{-1}$ ).

The formal statistical errors in the *Gaia* data are quite small and certainly much smaller e.g. than the actual deviations of the Milky Way kinematics (or most external galaxies) from the axisymmetry and steady-state assumptions. Moreover, the *Gaia* data set contains a very large number of values. In these situations, the formal statistical uncertainties become meaningless as the uncertainties become entirely dominated by systematics. This is a common issue also for the dynamical modelling of high- $S/N$  integral-field kinematics. To approximately account for systematic errors in the

<sup>2</sup> We use the Python version 5.0.2 of the `mgefit` package available from <https://pypi.org/project/mgefit/>

<sup>3</sup> We use the Python version 5.0.21 of the `jampy` package available from <https://pypi.org/project/jampy/>

data and approximations in the model assumptions we follow the approach of Sec. 3.2 of a previous modelling paper by van den Bosch & van de Ven (2009), as modified for Bayesian analysis in Sec. 6.1 of Mitzkus et al. (2017). First, after an initial fit, we adopt for the kinematics a constant error of  $\epsilon = 5.7 \text{ km s}^{-1}$  to give  $\chi^2/\text{DOF} = 1$ . Then we multiply  $\epsilon$  by  $(2N)^{0.25}$ . This is equivalent to changing the  $1\sigma$  confidence level from  $\Delta\chi^2 = 1$  to  $\Delta\chi^2 = \sqrt{2N}$ , which represents the standard deviation of the  $\chi^2$ .

JAM<sub>sph</sub> or JAM<sub>cyl</sub> uses as fixed input the density of the tracer population (Jurić et al. 2008) and a model for the gas density (McMillan 2017). The model has nine free parameters: (i) the velocity dispersion ratios or anisotropies ( $\sigma_\theta/\sigma_r$ <sup>4</sup> and  $\sigma_\phi/\sigma_r$ <sup>5</sup>) for both the flattest ( $q < 0.2$ ) Gaussian components (subscript 1) of the MGE and the rest (subscript 2), to allow for some of the observed clear spatial variation of the anisotropy, while keeping the model as simple as possible; (ii) the inner logarithmic slope of the gNFW profile ( $\alpha_{\text{DM}}$ ); (iii) the dark matter fraction  $f_{\text{DM}}$  within a sphere of radius  $R_\odot$ ; (iv) the mass-to-light ratio  $M_*/L_V$  of the stellar component in the V-band; (v) the axial ratio  $q$  and (vi) the scale radius ( $r_s$ ) of the dark matter profile.

The Bayesian modelling was performed using the `adamet`<sup>6</sup> package of Cappellari et al. (2013), which implements the Adaptive Metropolis algorithm by Haario et al. (2001). This is used to estimate the posterior distribution, as in standard MCMC methods (Gelman et al. 2013), to get the confidence levels of the best fitting parameters and to show the relations between the different parameters. We adopted constant priors on all parameters, in such a way that the probability of the model, given the data, is just the likelihood  $P(\text{data}|\text{model}) \propto \exp(-\chi^2/2)$ .

## 4 RESULTS

### 4.1 JAM fit to the Gaia data

Formally, the model has 9 free parameters, however, most of them are either directly constrained by the data or irrelevant and marginalized over. We include these 9 parameters are included just not to risk underestimating the model uncertainties. The four ratios between the different components of the velocity dispersion can be directly measured from the maps, while the  $M_*/L$  has an almost one-to-one correspondence to the dark matter fraction  $f_{\text{DM}}$ . The halo scale length  $r_s$  is totally unconstrained by the Gaia data and is degenerate with  $\alpha_{\text{DM}}$ : their combination simply defines the density total slope. While the halo axial ratio  $q$  is consistent with a spherical shape. This effectively leaves to the model the freedom to vary only the two parameters  $f_{\text{DM}}$  and  $\alpha_{\text{DM}}$ , which describe the dark matter halo, to fit a set of four two-dimensional kinematic maps!

The best-fitting model for the velocity maps is shown in Fig. 1. We also show for comparison the model without dark matter and the best-fitting model with a “standard” Navarro, Frenk and White (NFW)  $\alpha_{\text{DM}} = -1$  profile (Navarro et al.

1996). The median parameters from the posterior distribution for all three models are listed in Table 1 together with the  $1\sigma$  uncertainties, defined as half of the intervals enclosing 68 per cent of the posterior values, marginalized over the other parameters.

To estimate the effect of asymmetries in the kinematics we also fitted two models to two independent subsets of the Gaia data extracted from two azimuthal sectors ( $-15^\circ < \phi < 0^\circ$  and  $0^\circ < \phi < 15^\circ$ ) of our data. The results for the two sectors (Table 1) are consistent with each other and with the main model. As an extreme test of the sensitivity of our model to the assumptions on the orientation of the velocity ellipsoid, we also have fit a model (JAM<sub>cyl</sub>) which assumes a cylindrically-aligned velocity ellipsoid (Cappellari 2008). The JAM<sub>sph</sub> model gives a slightly better fit the data than JAM<sub>cyl</sub>, consistently with the finding that the Milky Way velocity ellipsoid is nearly spherical aligned (Hagen et al. 2019; Everall et al. 2019). However, the difference between the parameters inferred by two JAM<sub>sph</sub> and JAM<sub>cyl</sub> models is minimal as the two solutions are not very different in the disc plane.

Three results can be inferred from Fig. 1: (i) The most striking and important is how well this simple equilibrium model is able to capture the average Gaia kinematics. Here the main model residuals are due to the known  $\lesssim 10$  per cent non-equilibrium and non-axisymmetry features (Gaia Collaboration et al. 2018b), which cannot be described by an equilibrium model. (ii) It is clear that a model without dark matter completely fails to describe the observations, (iii) moreover, a standard NFW dark matter profile does not provide an equally good fit as the best-fitting one, with our median dark halo slope  $\alpha_{\text{DM}} = -1.53 \pm 0.12$ . In particular, an NFW halo systematically over-estimates  $\sigma_z$  and the radial gradient in  $v_\phi$ . The halo slope lies in the range expected from simple predictions for halo contractions (Gnedin et al. 2004) for samples of real galaxies (e.g. Fig. 2 in Cappellari et al. 2013). This is consistent with previous work indicating a steeper slope than the standard NFW is needed in the disc region of the Milky Way around the solar region (Portail et al. 2017; Cole & Binney 2017).

Our model has a total density at the solar position of  $\rho_{\text{tot}}(R_\odot) = 0.0640 \pm 0.0043 \text{ M}_\odot \text{ pc}^{-3}$  and a dark matter density of  $\rho_{\text{DM}}(R_\odot) = 0.0115 \pm 0.0020 \text{ M}_\odot \text{ pc}^{-3}$ , corresponding to a dark matter energy density of  $0.437 \pm 0.076 \text{ GeV cm}^{-3}$ . These values are broadly consistent with previous determinations (McKee et al. 2015; McMillan 2017).

The posterior distribution of the parameters for the gNFW model are shown in Fig. 2. This plot also shows the expected covariance between the mass-to-light ratio, the dark matter fraction and the inner slope of the halo: models with steeper (more negative)  $\alpha_{\text{DM}}$  have lower  $(M_*/L)_V$  ratio and higher dark-matter fraction  $f_{\text{DM}}$ . This distribution also shows that an NFW profile (red dashed line in Fig. 2) is outside the  $3\sigma$  confidence level. In addition, as comparison the blue shaded region indicates the stellar mass-to-light ratio from stellar counts  $0.75 \text{ M}_\odot/L_{\odot V}$  (15% uncertainty at  $1\sigma$  level from Flynn et al. 2006). This shows that our model  $(M_*/L)_V$  is consistent with the stellar-counts determination within the errors. Our model strongly excludes flattened halos and favour a nearly round one, consistent with recent Gaia results (Wegg et al. 2019).

<sup>4</sup> For JAM<sub>cyl</sub> this is  $\sigma_z/\sigma_R$

<sup>5</sup> For JAM<sub>cyl</sub> this is  $\sigma_\phi/\sigma_R$

<sup>6</sup> We use the Python version 2.0.7 of the `adamet` package available from <https://pypi.org/project/adamet/>

**Table 1.** Median parameters and 68per cent ( $1\sigma$ ) confidence intervals for the spherically or cylindrically-aligned JAM models

Parameter	Spherically-aligned JAM <sub>sph</sub>					Cylindrically-aligned JAM <sub>cyl</sub> gNFW Dark Halo
	No Dark Halo	NFW Dark Halo	gNFW Dark Halo	$-15^\circ < \phi < 0^\circ$	$0^\circ < \phi < 15^\circ$	
$\alpha_{DM}$	-	-1	$-1.53 \pm 0.12$	$1.52 \pm 0.13$	$-1.50 \pm 0.12$	$-1.48 \pm 0.13$
$f_{DM}$	-	$0.73 \pm 0.05$	$0.86 \pm 0.06$	$0.85 \pm 0.06$	$0.84 \pm 0.05$	$0.91 \pm 0.05$
$(\sigma_\theta/\sigma_r)_1$	$0.97 \pm 0.14$	$0.67 \pm 0.05$	$0.62 \pm 0.05$	$0.61 \pm 0.05$	$0.60 \pm 0.05$	$0.63 \pm 0.04$ 4
$(\sigma_\theta/\sigma_r)_2$	$0.82 \pm 0.11$	$0.75 \pm 0.08$	$0.71 \pm 0.09$	$0.76 \pm 0.10$	$0.73 \pm 0.11$	$0.83 \pm 0.06$ 4
$(\sigma_\phi/\sigma_r)_1$	$0.87 \pm 0.20$	$0.79 \pm 0.08$	$0.80 \pm 0.08$	$0.78 \pm 0.09$	$0.77 \pm 0.08$	$0.80 \pm 0.07$ 5
$(\sigma_\phi/\sigma_r)_2$	$0.87 \pm 0.20$	$0.94 \pm 0.12$	$0.93 \pm 0.12$	$0.95 \pm 0.15$	$0.97 \pm 0.14$	$0.96 \pm 0.13$ 5
$(M_*/L)_V$	$1.82 \pm 0.03$	$0.58 \pm 0.12$	$0.30 \pm 0.13$	$0.34 \pm 0.13$	$0.38 \pm 0.13$	$0.26 \pm 0.12$
$r_s$ [kpc]	-	$10.8 \pm 1.0$	$16.8 \pm 5.4$	$17.2 \pm 5.3$	$17.1 \pm 5.4$	$16.2 \pm 5.2$
$q$	-	$1.16 \pm 0.25$	$1.14 \pm 0.21$	$1.12 \pm 0.23$	$1.33 \pm 0.31$	$1.40 \pm 0.35$
$\chi^2$	10610	3749	3326	3490	3453	3480
$\chi^2/\text{DOF}$	3.25	1.15	1.02	1.07	1.06	1.07

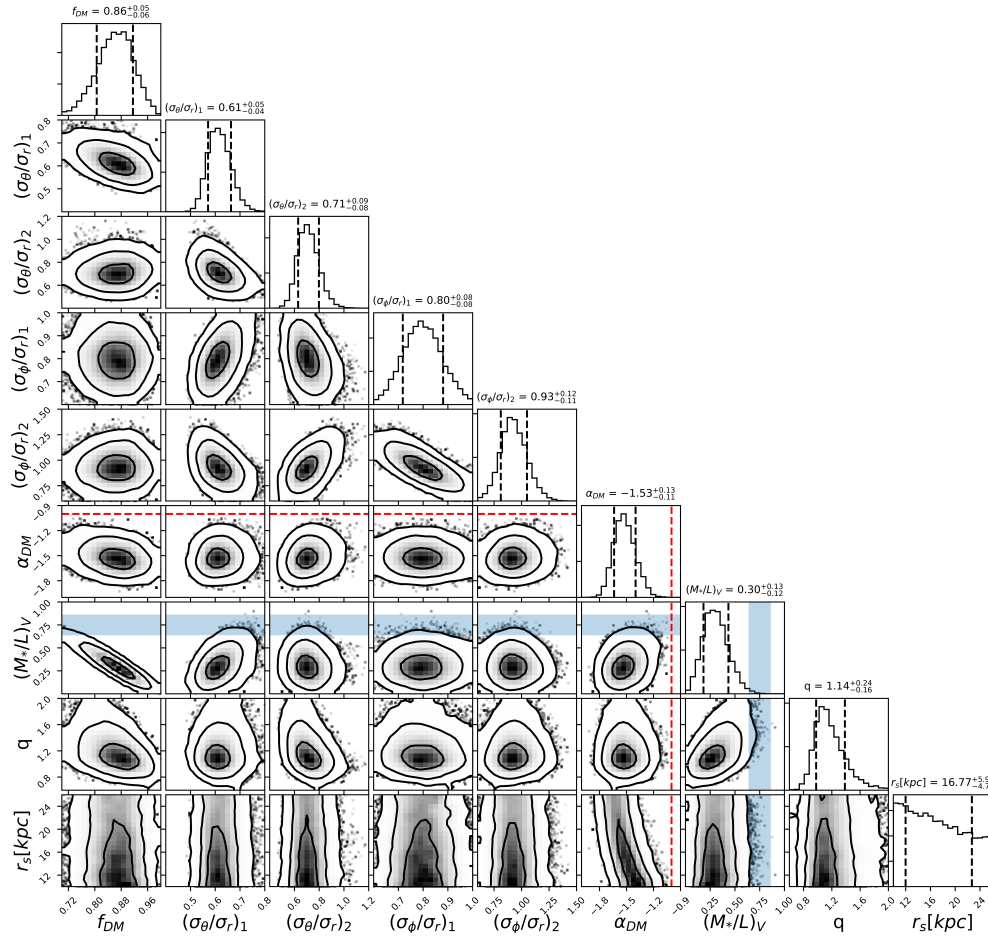


**Figure 2. gNFW parameters corner plot.** Each panel shows the posterior probability distribution marginalized over two dimensions (contours) and one dimension (histograms). The parameters are (i) the dark matter fraction  $f_{DM}$  inside a sphere of radius  $R_\odot = 8.2$  kpc; (ii) the velocity dispersion ratios  $[(\sigma_\theta/\sigma_r)_1, (\sigma_\phi/\sigma_r)_1]$  of the Gaussians flatter than  $q = b/a = 0.2$  and the rest  $[(\sigma_\theta/\sigma_r)_2, (\sigma_\phi/\sigma_r)_2]$ ; (iii) the inner dark matter halo logarithmic slope  $\alpha_{DM}$ , (iv) the stellar mass-to-light ratio  $(M_*/L)_V$ ; (v) the axial ratio  $q$  of the dark matter halo and (vi) the scale radius  $r_s$  for the dark matter halo. The thick contours represent the 1, 2 and  $3\sigma$  confidence levels for one degree of freedom. The red dashed line marks the “standard”  $\alpha_{DM} = -1$  slope of the Navarro, Frenk and White (NFW) (Navarro et al. 1996) dark matter profile and the blue shaded band indicates a mass-to-light ratio estimate from stellar counts (Flynn et al. 2006). The numbers with errors on top of each plot are the median (black dashed lines) and 16th and 84th percentiles of the posterior for each parameter, marginalized over the other parameters.

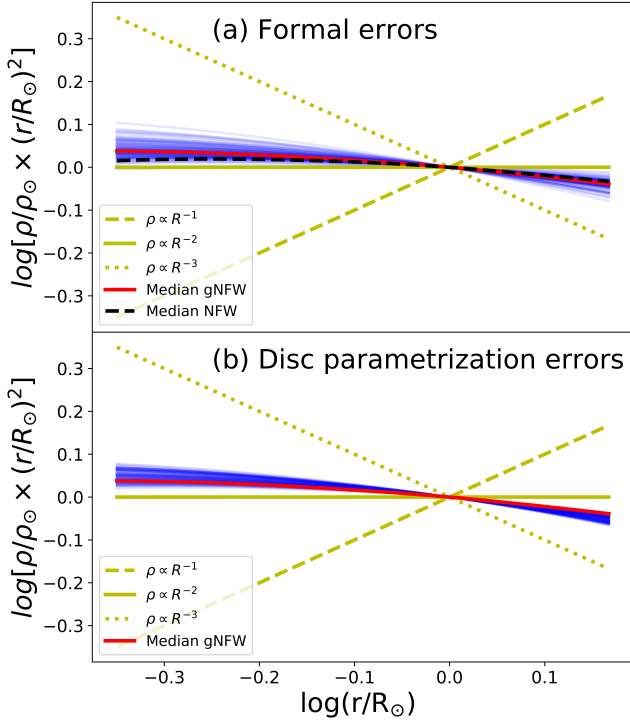


**Figure 3. Milky Way total density profile.** (a) The blue shaded region shows 100 realizations of the density profile from the model posterior of Fig. 2. The black line is the median density for the NFW  $\alpha_{\text{DM}} = -1$  model. (b) Density profiles obtained by randomly varying the assumed parametrization for the stellar disc (Jurić et al. 2008) within the quoted errors and re-running the whole model fitting procedure.

#### 4.2 Total density profile

Having found our best-fitting model we can find the total density profile, using the `mge_radial_density` procedure in the `jumpy` package (see footnote 3).

The *total*-density distribution is the quantity that the dynamical models directly measure. This is very tightly constrained by the *Gaia* data and it is shown in Fig. 3. From the posterior of the models we measure a total density mean logarithmic slope of  $\alpha_{\text{tot}} \equiv \Delta \log \rho_{\text{tot}} / \Delta \log r = -2.149 \pm 0.055$  in the radial range 3.6–12 kpc of the data. These radii correspond to about 0.9–2.9 half-light radii  $R_{\text{e}}^{\text{max}}$ , for our measured<sup>7</sup>  $R_{\text{e}}^{\text{max}} \approx 4.122$  kpc. The measured total-density slope is consistent with the “universal” slope  $\alpha_{\text{tot}} \approx -2.19 \pm 0.03$  inferred at comparable radii on early-type disc galaxies (Cappellari et al. 2015) with effective velocity dispersion not smaller than the Milky Way’s value (Kormendy & Ho 2013)  $\sigma_{\text{e}} = 105 \pm 20$  km s<sup>-1</sup>.

We also investigate how much the uncertainties of the parametrization of the Milky Way stellar tracer distribution affect our JAM<sub>sph</sub> results. For this, we vary the disc parameters of Jurić et al. (2008) within the quoted errors and then redo the JAM<sub>sph</sub> fit using the `capfit` least-

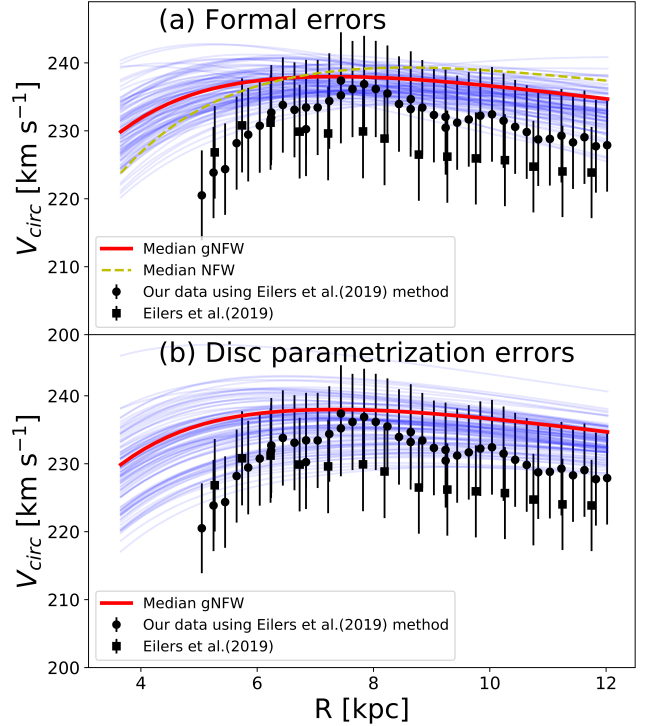


**Figure 4. Circular Velocity with formal and disc parametrization errors.** The red line is the circular velocity of our median gNFW model, the black squares are the recent measurements of Eilers et al. (2019), the black points are derived with our data and the Eilers et al. (2019) method and the yellow dashed line is the for the mean normal NFW profile. The blue lines in panel (a) are the circular velocities of 100 random parameters of the posterior distribution that give the formal error from the fit and in panel (b) they are 100 different disc models that give the systematic error due to disc parametrization.

squares program<sup>8</sup>. This is repeated for 100 different disc models, for random values of the scale heights, scale lengths and the fraction of the thick disc normalization, within the given 20 per cent  $1\sigma$  uncertainties (Jurić et al. 2008). The result for the total density can be seen in panel (b) of Fig. 3. Here the blue lines indicate the systematic error due to the Milky Way stellar tracer model. This gives us an alternative estimate of the value and systematic error  $\alpha_{\text{tot}} \equiv \Delta \log \rho_{\text{tot}} / \Delta \log r = -2.194 \pm 0.044$  and the logarithmic slope of the gNFW profile is  $\alpha_{\text{DM}} = -1.455 \pm 0.055$ , which is comparable to the previous estimate.

During this testing of these systematic errors, we saw that higher values for the scale height and length of our disc models seem to give JAM models that agree even better with our data. We leave further exploration of this aspect to a subsequent study.

<sup>7</sup> Using `mge_half_light_isophote` in the JAM package.

### 4.3 Circular velocity curve

Having found a model that describes our *Gaia* data we can also derive the circular velocity, using the `mge_vcirc` procedure in the `jampy` package (see footnote 3).

The circular velocity of the Milky Way disc region is plotted as a red line for the gNFW and as a dashed yellow line for the normal NFW profile in panel (a) of Section 4.3. The black points are derived with our data when using the same non-parametric method of Eilers et al. (2019), also based on the axisymmetric Jeans equations, to calculate the circular velocity and the black squares are the measurements of Eilers et al. (2019). The small offset between our values and the previous work by Eilers et al. (2019) is coming from our slightly higher value of the solar velocity because of the newest Abuter et al. (2019) results for the distance to the Galactic center. Reassuringly, the two circular velocities are consistent within the estimated quite small systematic uncertainties. The model with NFW halo would produce an inconsistent circular velocity, supporting the finding that this is excluded by the *Gaia* data.

The blue transparent lines are 100 random realizations for the circular velocity from the posterior distribution that indicates the formal uncertainty for our mean circular velocity but include our approximate treatment for systematics by scaling the input kinematic errors. At the solar position we get a value of  $v_{\text{circ}}(R_{\odot}) = 236.5 \pm 1.8 \text{ km s}^{-1}$ . This value also agrees well with the value of Eilers et al. (2019) ( $229.0 \pm 0.2 \text{ km s}^{-1}$ ), where they use a quite different stellar sample, stellar distance estimates and modelling assumptions, and with another recent work by Mróz et al. (2019) ( $233.6 \pm 2.8 \text{ km s}^{-1}$ ) in which they construct the rotation curve of the Milky Way using the proper motion and radial velocities from *Gaia* for classical Cepheids.

The result for the effect of the uncertainties of the parametrization of the Milky Way stellar tracer distribution on the circular velocity can be seen in panel (b) of Section 4.3. Here the blue lines indicate the systematic error due to the Milky Way stellar tracer model. This gives us an alternative estimate of the value and systematic error  $v_{\text{circ}}(R_{\odot}) = 236.3 \pm 3.1 \text{ km s}^{-1}$ , which is comparable to the previous estimate.

## 5 CONCLUSION

The model presented is the first stringent test of the Newtonian equations of motion on galactic scales. It demonstrates that we already have a remarkably accurate knowledge of the mass distribution in our Milky Way and we can concisely describe the main average characteristics of the observed stellar kinematics with a minimal set of assumptions. The model also shows that the average kinematics of the Milky Way, outside of the bar region, can be well described by an axisymmetric and equilibrium model. The fact that we can well describe the Galactic kinematics, regardless of relatively minor deviations from equilibrium and axisymmetry (Widrow et al. 2012; Gaia Collaboration et al. 2018b;

Antoja et al. 2018), is consistent with observations of external galaxies, where such deviations are widespread, but models can still capture the average kinematic properties (Cappellari et al. 2013) and recover circular velocity profiles to 10% accuracy (Leung et al. 2018), even from data of much inferior quality.

The *Gaia* data are going to improve in accuracy with subsequent data releases. Moreover, when not relying entirely on parallactic distances, one can significantly increase the extent of the region where kinematics can be measured (Wegg et al. 2019). Dynamical models will soon be able to study our Galaxy’s density distribution over larger distances. These models are starting to provide a description of the dynamics of the Milky Way at a level that is impossible to achieve in external galaxies. This is providing a key benchmark for our knowledge of galactic dynamics that will complement much less detailed studies of much larger samples of external galaxies.

## ACKNOWLEDGEMENTS

M.S. Nitschai warmly thanks the two scholarships, ‘DAAD-PROMOS-Stipendium’ and ‘Baden-Württemberg-STIPENDIUM’, for the financial support during the stay abroad working on this project and the Astrophysics Department of the University of Oxford for the hospitality during that time. N.N. acknowledges support by Sonderforschungsbereich SFB 881 ‘The Milky Way System’ (subproject B8) of the German Research Foundation (DFG).

## REFERENCES

- Abuter R., et al., 2019, A&A submitted, [p. arXiv:1904.05721](#)
- Antoja T., et al., 2018, *Nature*, **561**, 360
- Binney J., Mamon G. A., 1982, *MNRAS*, **200**, 361
- Bissantz N., Gerhard O., 2002, *MNRAS*, **330**, 591
- Bland-Hawthorn J., Gerhard O., 2016, *ARA&A*, **54**, 529
- Bovy J., Leung H. W., Hunt J. A. S., Mackereth J. T., Garcia-Hernandez D. A., Roman-Lopes A., 2019, *MNRAS* submitted, [p. arXiv:1905.11404](#)
- Cappellari M., 2002, *MNRAS*, **333**, 400
- Cappellari M., 2008, *MNRAS*, **390**, 71
- Cappellari M., 2016, *ARA&A*, **54**, 597
- Cappellari M., 2017, *MNRAS*, **466**, 798
- Cappellari M., 2019, *MNRAS* submitted, [p. arXiv:1907.09894](#)
- Cappellari M., et al., 2006, *MNRAS*, **366**, 1126
- Cappellari M., et al., 2013, *MNRAS*, **432**, 1709
- Cappellari M., et al., 2015, *ApJ*, **804**, L21
- Cole D. R., Binney J., 2017, *MNRAS*, **465**, 798
- Courteau S., et al., 2014, *Reviews of Modern Physics*, **86**, 47
- Eilers A.-C., Hogg D. W., Rix H.-W., Ness M. K., 2019, *ApJ*, **871**, 120
- Emsellem E., Monnet G., Bacon R., 1994, *A&A*, **285**, 723
- Everall A., Evans N. W., Belokurov V., Schönrich R., 2019, *MNRAS*, **489**, 910
- Flynn C., Holmberg J., Portinari L., Fuchs B., Jahreiß H., 2006, *MNRAS*, **372**, 1149
- Gaia Collaboration et al., 2016, *A&A*, **595**, A1
- Gaia Collaboration et al., 2018a, *A&A*, **616**, A1
- Gaia Collaboration et al., 2018b, *A&A*, **616**, A11
- Gebhardt K., et al., 2000, *AJ*, **119**, 1157
- Gelman A., Carlin J., Stern H., Dunson D., Vehtari A., Rubin D., 2013, *Bayesian Data Analysis*, Third Edition. Chapman

<sup>8</sup> This is part of the Python package `pPXF` by Cappellari (2017) available here <https://pypi.org/project/ppxf/>

- & Hall/CRC Texts in Statistical Science, Taylor & Francis,  
<https://books.google.co.uk/books?id=ZXL6AQAAQBAJ>
- Gerhard O. E., 1993, *MNRAS*, **265**, 213
- Gnedin O. Y., Kravtsov A. V., Klypin A. A., Nagai D., 2004, *ApJ*, **616**, 16
- Haario H., Saksman E., Tamminen J., 2001, *Bernoulli*, **7**, 223
- Hagen J. H. J., Helmi A., de Zeeuw P. T., Posti L., 2019, *A&A*, **629**, A70
- Jeans J. H., 1922, *MNRAS*, **82**, 122
- Jin Y., Zhu L., Long R. J., Mao S., Xu D., Li H., van de Ven G., 2019, *MNRAS*, **486**, 4753
- Joshi Y. C., 2007, *MNRAS*, **378**, 768
- Jurić M., et al., 2008, *ApJ*, **673**, 864
- Kafle P. R., Sharma S., Lewis G. F., Bland-Hawthorn J., 2014, *ApJ*, **794**, 59
- Klypin A. A., Trujillo-Gomez S., Primack J., 2011, *ApJ*, **740**, 102
- Kormendy J., Ho L. C., 2013, *ARA&A*, **51**, 511
- Krajinović D., Cappellari M., Emsellem E., McDermid R. M., de Zeeuw P. T., 2005, *MNRAS*, **357**, 1113
- Lablanche P.-Y., et al., 2012, *MNRAS*, **424**, 1495
- Leung G. Y. C., et al., 2018, *MNRAS*, **477**, 254
- Li H., Li R., Mao S., Xu D., Long R. J., Emsellem E., 2016, *MNRAS*, **455**, 3680
- McKee C. F., Parravano A., Hollenbach D. J., 2015, *ApJ*, **814**, 13
- McMillan P. J., 2017, *MNRAS*, **465**, 76
- Mitzkus M., Cappellari M., Walcher C. J., 2017, *MNRAS*, **464**, 4789
- Mróz P., et al., 2019, *ApJ*, **870**, L10
- Navarro J. F., Frenk C. S., White S. D. M., 1996, *ApJ*, **462**, 563
- Portail M., Gerhard O., Wegg C., Ness M., 2017, *MNRAS*, **465**, 1621
- Posti L., Helmi A., 2019, *A&A*, **621**, A56
- Reid M. J., et al., 2009, *ApJ*, **700**, 137
- Rix H.-W., de Zeeuw P. T., Cretton N., van der Marel R. P., Carollo C. M., 1997, *ApJ*, **488**, 702
- Rybicki G. B., 1987, in de Zeeuw P. T., ed., *IAU Symposium Vol. 127, Structure and Dynamics of Elliptical Galaxies*. D. Reidel, Dordrecht, p. 397, [doi:10.1007/978-94-009-3971-4\\_41](https://doi.org/10.1007/978-94-009-3971-4_41)
- Schönrich R., Binney J., Dehnen W., 2010, *MNRAS*, **403**, 1829
- Schönrich R., McMillan P., Eyer L., 2019, *MNRAS*, **485**, 3296
- Schwarzschild M., 1979, *ApJ*, **232**, 236
- Valluri M., Merritt D., Emsellem E., 2004, *ApJ*, **602**, 66
- Vogelsberger M., et al., 2014, *Nature*, **509**, 177
- Watkins L. L., van der Marel R. P., Bellini A., Anderson J., 2015, *ApJ*, **812**, 149
- Watkins L. L., van der Marel R. P., Sohn S. T., Evans N. W., 2019, *ApJ*, **873**, 118
- Wegg C., Gerhard O., Portail M., 2015, *MNRAS*, **450**, 4050
- Wegg C., Gerhard O., Bieth M., 2019, *MNRAS*, **485**, 3296
- Widrow L. M., Gardner S., Yanny B., Dodelson S., Chen H.-Y., 2012, *ApJ*, **750**, L41
- Wytke J. S. B., Turner E. L., Spergel D. N., 2001, *ApJ*, **555**, 504
- de Lorenzi F., et al., 2009, *MNRAS*, **395**, 76
- van de Ven G., van den Bosch R. C. E., Verolme E. K., de Zeeuw P. T., 2006, *A&A*, **445**, 513
- van den Bosch R. C. E., van de Ven G., 2009, *MNRAS*, **398**, 1117
- van der Marel R. P., 1991, *MNRAS*, **253**, 710
- van der Marel R. P., Franx M., 1993, *ApJ*, **407**, 525
- van der Marel R. P., Cretton N., de Zeeuw P. T., Rix H.-W., 1998, *ApJ*, **493**, 613

This paper has been typeset from a  $\text{\LaTeX}$  file prepared by the author.